Asian Journal of Chemistry; Vol. 38, No. 7 (2026), 1862-1872
ASIAN JOURNAL OF CHEMISTRY
https://doi.org/10.14233/ajchem.2026.36068

Synthesis of Three Ru(II) Polypyridyl Complexes of 2-(4-(Pyrrolidine-1-yl)phenyl)-1*H*-imidazo[4,5-*f*][1,10]phenanthroline: Characterisation, DNA Binding, Antimicrobial and Cytotoxicity Studies

MARKANDEYA NAMANI[1,*] and NAVANEETHA NAMBIGARI[1,2]

[1]Department of Chemistry, NTR Government Degree College for Women (A), Palamuru University, Mahabubnagar-509001, India
[2]Department of Chemistry, University College of Science, Saifabad, Osmania University, Hyderabad-500004, India

*Corresponding author: E-mail: namanimark79@gmail.com

Received: 25 March 2026 *Accepted*: 9 June 2026 *Published online*: 3 July 2026 AJC-22412

Three Ru(II) complexes having general formula, $[Ru(A)_2PPIP](ClO_4)_2 \cdot 2H_2O$, where PPIP = 2-(4-(pyrrolidine-1-yl)phenyl)-1*H*-imidazo[4,5-*f*]-[1,10]phenanthroline and A = phen = 1,10 phenanthroline (**1**), bpy = bipyridine (**2**), dmb = 4,4′-dimethyl 2,2′-bipyridine (**3**) were synthesised. In order to conduct the structural investigation of these complexes, various techniques such as ^{1}H NMR, ^{13}C NMR, FT-IR, ESI mass and UV-visible were utilised. The Ru(II) complexes were confirmed to have an octahedral geometry based on the spectroscopic and analytical results. Their interaction with DNA was systematically investigated using UV-Vis absorption, fluorescence quenching and viscosity measurements, all of which consistently indicated an intercalative binding mode. The agreement among these techniques strengthens the proposed DNA-binding mechanism. Furthermore, DNA cleavage studies revealed that all the three Ru(II) complexes effectively converted supercoiled DNA (Form I) into nicked circular DNA (Form II), demonstrating their significant DNA-cleaving capability. *In vitro* biological evaluations against both Gram-positive and Gram-negative microbial strains revealed that the Ru(II) complexes exhibited superior antimicrobial activity compared with the PPIP ligand. Cytotoxicity studies further demonstrated that the Ru(II) complexes were more potent than the free ligand, while showing enhanced activity relative to the reference standards. In addition, molecular modelling investigations were performed to elucidate their geometric and electronic characteristics. The electrostatic potential surface contours for the complexes were also analysed to obtain the insights into the charge distribution and their nucleophilic level of sensitivity.

Keywords: Ruthenium(II) complexes, Phenanthroline, Bipyridine, DNA binding, Intercalation, Photocleavage, Biological activity.

INTRODUCTION

Metal-based compounds offer unique opportunities for the design of therapeutic agents that are not readily accessible with organic molecules, making this an increasingly prominent field of study. As a result of their extensive variety of coordination numbers and geometries, accessible redox states, thermodynamic and kinetic properties and the inherent features of both the cationic metal ion and the ligand, medicinal chemists have access to a broad spectrum of reactivities. Since the pivotal discovery of the biological activity of cisplatin [1-10], the potential of metal-based anticancer drugs has been fully realised and exploited, despite metals having been used therapeutically for a considerable time in a more or less empirical manner [11-15].

Cisplatin remains one of the most successful and widely used chemotherapeutic agents in clinical oncology, exhibiting remarkable efficacy, particularly in the treatment of testicular cancer, where early diagnosis can result in cure rates approaching 100%. Following its unforeseen discovery and subsequent development as an anticancer drug [16-20], considerable attention has been directed toward other platinum-group metal complexes. Among platinum-group metal complexes, ruthenium compounds have emerged as promising therapeutic candidates due to their favourable biological properties. In addition to their roles as biological stains and calcium channel inhibitors, they exhibit remarkable antibacterial, antiparasitic and anticancer activities. Their broad biological potential has supported various biotechnological applications, while their antimicrobial properties highlight their promise as alternatives or adjuncts to conventional antibiotics in combating antimicrobial resistance [21-26].

Despite extensive studies on Ru(II) polypyridyl complexes as DNA-targeting agents, many existing systems suffer from limited selectivity, moderate DNA-binding affinity and suboptimal cellular uptake, which constrain their therapeutic efficacy [27]. Furthermore, most reported intercalating ligands lack strong electron-donating substituents capable of modulating the metal center's redox potential and enhancing hydrophobic interactions with DNA base pairs [28]. To address these limitations, the novel ligand, 2-(4-(pyrrolidin-1-yl)phenyl)-1*H*-imidazo[4,5-*f*]phenanthroline (PPIP) was designed, incorporating a pyrrolidine-substituted phenyl ring. The electron-rich pyrrolidine group is expected to enhance DNA intercalation through extended π-conjugation and increased planarity, while also improving the lipophilicity and cellular permeability of the resulting Ru(II) complexes compared to traditional phenanthroimidazole derivatives. This work addresses the limitations of existing Ru(II) systems by incorporating a tailored intercalating ligand with enhanced DNA-binding affinity and favourable physico-chemical properties. Thus, three new Ru(II) polypyridyl complexes were synthesised and characterised. DNA-binding studies were carried out using UV-Vis, fluorescence and viscosity techniques. Molecular modeling investigations were also performed to evaluate the geometric and electronic properties of the complexes, while the electrostatic potential surface analysis was conducted to assess their nucleophilic reactivity.

EXPERIMENTAL

All chemicals and solvents were obtained from the reputed commercial sources like Sigma-Aldrich, Merck, HiMedia and Finar) and used without further purification. Calf thymus DNA (*ct*-DNA) and pBR322 DNA were procured from Genei (Bangalore, India). DNA-binding studies were performed in Tris-HCl buffer (5 mM Tris-HCl, 50 mM NaCl, pH 7.2). The purity and concentration of *ct*-DNA were determined spectrophotometrically using the A260/A280 ratio and a molar absorptivity of 6600 M^{-1} cm^{-1} at 260 nm. Stock solutions of DNA and complexes were freshly prepared in buffer and DMSO, respectively. ^1H and ^{13}C NMR spectra were recorded on a Bruker AV-400 spectrometer. FT-IR spectra were obtained using a Perkin-Elmer 1605 FT-IR spectrophotometer, while elemental analyses were performed on a Perkin-Elmer 240 analyzer. ESI-MS measurements were carried out using a VG AUTOSPEC mass spectrometer. Electronic absorption spectra were recorded on a Shimadzu UV-2600 spectrophotometer, and fluorescence studies were conducted using a JASCO Cary Eclipse spectrofluorometer.

Synthesis of the intercalated ligand (PPIP) and its Ru(II) complexes

Synthesis of PPIP ligand: 2-(4-(Pyrrolidin-1-yl)phenyl)-1*H*-imidazo[4,5-*f*][1,10]phenanthroline (PPIP) ligand was synthesised using phendione (0.53 g, 2.5 mmol), 4-(1-pyrrolidine)-benzaldehyde (0.613 g, 3.5 mmol) and ammonium acetate (3.86 g, 50 mmol), which upon dissolving in glacial acetic acid (15 mL) and refluxed for 5 h (**Scheme-I**). A brick-red solution was cooled to room temperature. Distilled water and concentrated ammonia solution were added dropwise to this solution, resulting in the formation of an orange-yellow precipitate, which was washed and dried. Yield: 64.3%: Elemental anal. of $C_{23}H_{19}N_5$: calcd. (found) %: C, 75.59 (75.61); H, 5.24 (5.25); N, 19.16 (19.13); ES^+-MS calcd.: 365.9; found: 366.9; IR (KBr, ν_{max}, cm^{-1}): 3462 (N-H), 1602 (C=C), 1525 (C=N), 1070 (C-N), 811 (C-H); ^1H NMR (DMSO-d_6, 400 MHz, δ ppm): 9.14 (d, 2H), 9.05 (d, 2H), 8.82 (d, 2H), 8.41 (d, 2H), 7.97 (d, 2H), 7.41(s, 1H), 2.01 (m, 4H), 1.95 (m, 4H); ^{13}C NMR (100 MHz, DMSO-d_6, δ ppm): 151.91, 148.42, 147.52, 139.71, 129.33, 128.49, 127.46, 123.11, 116.62, 111.53, 47.34, 25.01.

Synthesis of $[Ru(phen)_2(PPIP)](ClO_4)_2\cdot 2H_2O$ (complex 1): A solution of *cis*-$[Ru(Phen)_2Cl_2]\cdot 2H_2O$ (phen = 1,10 phenanthroline, 0.5 mmol, 0.284 g) and PPIP ligand (0.5 mmol, 0.182 g) in ethanol (15 mL) was refluxed at 120 ºC for 14 h with a nitrogen purge. Upon cooling the light purple solution to room temperature, a saturated aqueous $NaClO_4$ solution was swiftly mixed. The resulting crimson solution was collected, washed with diethyl ether, ethanol followed by water and subsequently dried using a vacuum (**Scheme-I**). Yield: 64.3%; Elemental anal. of $C_{47}H_{35}N_9Ru$: calcd. (found) %: C, 77.72 (77.76); H, 4.86 (4.88), N, 17.37 (17.35); ES^+-MS calcd.: 413.1, found: 414.7; IR (KBr, ν_{max}, cm^{-1}): 3588 (N-H), 1525 (C=N), 1608 (C=C), 1088 (C-N), 844 (C-H), 622 (Ru-N); ^1H NMR (DMSO-d_6, 400 MHz, δ ppm): 8.78 (d, 4H), 8.72 (d, 2H), 8.31 (d, 4H), 8.21 (m, 4H) 8.12 (d, 2H), 7.97 (s, 2H), 7.76 (m, 2H), 3.37 (m, 4H), 1.92 (m, 4H); ^{13}C NMR (100, MHz, DMSO-d_6, δ ppm): 158.74, 156.57, 152.37, 151.42, 149.9, 148.6, 139.2, 129.2, 125.2, 121.5, 47.34, 25.01.

Synthesis of $[Ru(bpy)_2(PPIP)](ClO_4)_2\cdot 2H_2O$ (complex 2): A mixture of *cis*-$[Ru(bpy)_2Cl_2]\cdot 2H_2O$ (bpy = bipyridine, 0.5 mmol, 0.260 g) and PPIP ligand (0.5 mmol, 0.182 g) was prepared in ethanol (15 mL) and refluxed at 120 ºC for 14 h under a continuous N_2 gas purge to ensure an inert atmosphere. The reaction mixture turned light purple during reflux indicating complex **2** formation. After the completion of the reaction, the solution was cooled to room temperature. A saturated aqueous $NaClO_4$ solution was added dropwise to the cooled reaction mixture with continuous vigorous stirring, resulting in the formation of a red precipitate. The product was collected by filtration, thoroughly washed with small portions of water, ethanol and diethyl ether to remove residual impurities and finally dried under vacuum. Yield: 62.3%; Elemental anal. of $C_{43}H_{35}N_9Ru$: calcd. (found) %: C, 76.20 (76.21); H, 5.20 (5.22); N, 18.60 (18.62); ESI-MS (*m/z*): calcd. 389.6, found; 390.1; IR (KBr, ν_{max}, cm^{-1}): 3589 (N-H), 1526 (C=N), 1086 (C-N), 830 (C-H), 622 (Ru-N); ^1H NMR (DMSO-d_6, 400 MHz, δ ppm): 9.10 (d, 2H), 8.89 (d, 4H), 8.84 (d, 2H), 8.22 (t, 4H), 8.11 (t, 2H), 7.92 (m, 4H), 7.84 (d, 2H), 7.64 (d, 2H), 7.34 (m, 3H), 3.35 (m, 4H), 2.25 (m, 4H); ^{13}C NMR (100, MHz, DMSO-d_6, δ ppm): 156.80, 156.24, 156.33, 157.51, 149.72, 137.99, 137.85, 127.81, 124.51, 45.97, 28.98.

Synthesis of $[Ru(dmb)_2(PPIP)](ClO_4)_2\cdot 2H_2O$ (complex 3): A mixture of *cis*-$[Ru(dmb)_2Cl_2]\cdot 2H_2O$ (dmb = 4,4′-dimethyl-2,2′-bipyridine, 0.5 mmol, 0.288 g) and ligand PPIP (0.5 mmol, 0.182 g) was dissolved in ethanol (15 mL) and refluxed at 120 ºC for 14 h under a continuous N_2 gas purge to maintain an inert atmosphere and prevent oxidation. During reflux, the reaction mixture gradually developed a faint purple colour, indicating coordination of the PPIP

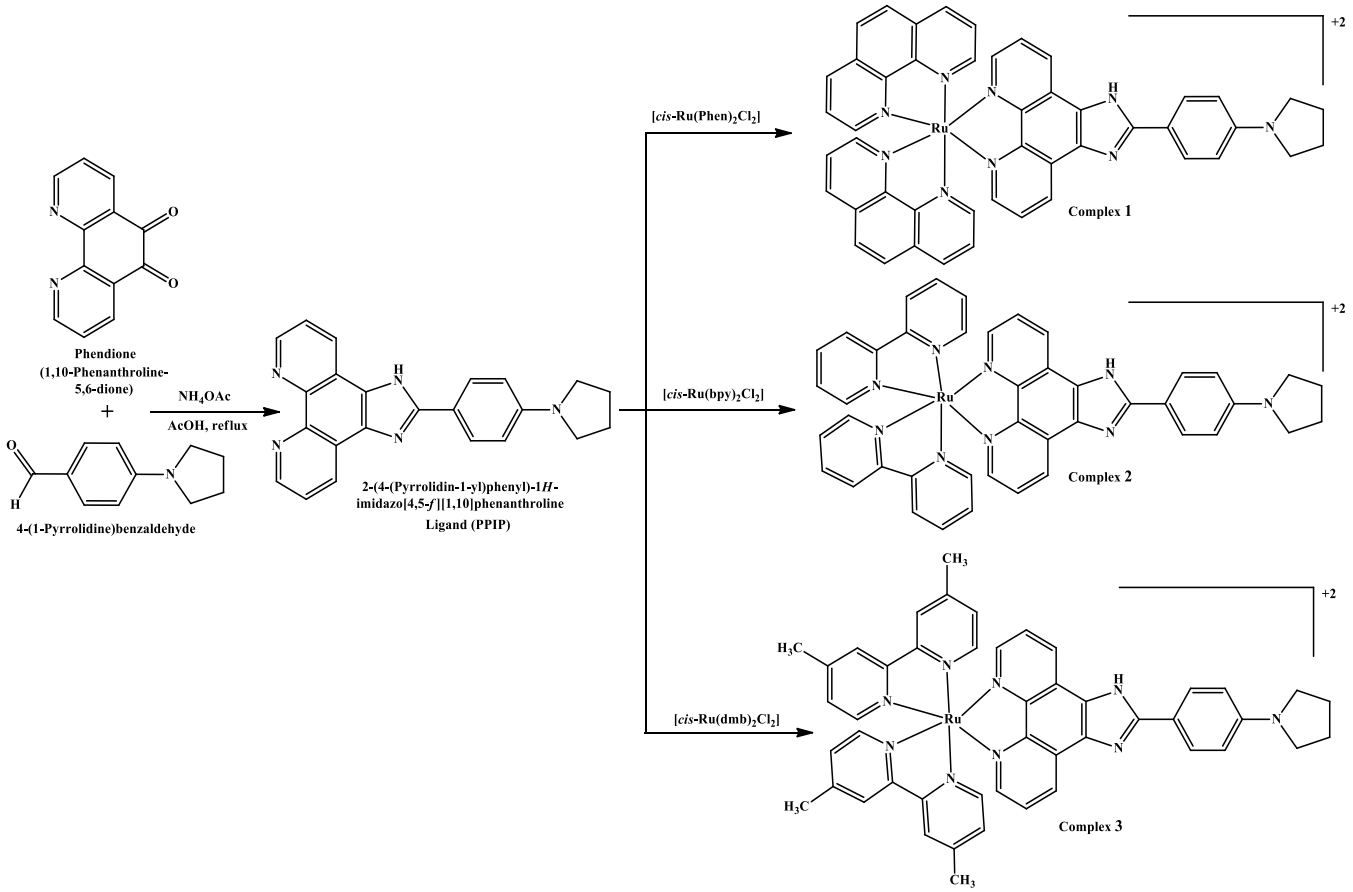

Scheme-I: Schematic representation of the synthetic route of complexes, $[Ru(phen)_2PPIP]^{2+}$ (**1**), $[Ru(bpy)_2PPIP]^{2+}$ (**2**) and $[Ru(dmb)_2PPIP]^{2+}$ (**3**)

ligand to the ruthenium precursor. After completion of the reaction, the mixture was cooled to room temperature. A saturated aqueous $NaClO_4$ solution was then added dropwise with continuous stirring, resulting in the formation of a red precipitate. The product was collected by filtration, washed thoroughly with water, ethanol and diethyl ether to remove residual impurities and finally dried under vacuum. Yield: 62.3%; Elemental anal. of $C_{47}H_{43}N_9Ru$: calcd. (found) %: C, 76.92 (76.90); H, 5.91 (5.92); N, 17.18 (17.16); ESI-MS (*m/z*): calcd. 417.5, found; 418.8; IR (KBr, ν_{max}, cm^{-1}): 3589 (N-H), 1608 (C=C), 1527 (C=N), 1075 (C-N), 823 (C-H), 622 (Ru-N); ^1H NMR (DMSO-d_6, 400 MHz, δ ppm): 9.09 (d, 2H), 8.74 (d, 4H), 8.71 (m, 6H), 8.22 (t, 4H), 8.14 (t, 2H), 8.06 (m, 4H), 7.55 (d, 4H), 7.42 (d, 3H), 7.16 (m, 3H), 2.50 (m, 4H), 1.91 (m, 4H); ^{13}C NMR (100, MHz, DMSO-d_6, δ ppm): 157.32, 156.58, 156.33, 151.51, 151.44, 149.72, 137.99, 129.53, 127.81, 124.51, 119.08, 46.03, 32.13.

Conformational optimisation of ligand and its Ru(II) complex: The DFT calculations were performed with Gaussian 09 package. Initially, the molecules were subjected to optimisation using the Semi-empirical PM_6 method in the gas phase. The HOMO-LUMO transitions between the different orbitals were evaluated with DFT using the B3LYP basis set for atoms C, H, N & Ru atom in a vacuum, for equilibrium geometry at the ground state. The molecular geometry, the highest occupied molecular orbital (HOMO), the lowest unoccupied molecular orbital (LUMO) energies were determined from optimised geometry (in gas).

RESULTS AND DISCUSSION

FT-IR studies: The FT-IR spectrum of the PPIP ligand exhibited characteristic bands at 3462, 1070 and 811 cm^{-1}, corresponding to N–H, C–N, and aromatic C–H vibrations, respectively. Pyridine C–H vibrations appeared in the range 733-721 cm^{-1}, while aromatic C–H vibrations were observed between 844 and 811 cm^{-1}. Upon complexation, these bands shifted to higher frequencies by approximately 20-30 cm^{-1}, indicating coordination of the ligand to the Ru(II) center. The complexes displayed characteristic C=C and C=N stretching bands in 1629-1608 and 1527-1525 cm^{-1}, respectively [29,30]. A new band at ~622 cm^{-1} was assigned to Ru–N stretching vibrations, confirming metal-ligand coordination and supporting an octahedral geometry around the Ru(II) ion. Enhanced 1,10-phenanthroline-associated bands were observed in the 1640-1420 cm^{-1} (Table-1).

^1H and ^{13}C NMR studies: The ^1H NMR spectra of the Ru(II) complexes showed significant changes in chemical shift values compared with the free PPIP ligand, confirming coordination. The proton resonances of the PPIP ligand appeared in the range of δ 1.9-8.8 ppm, while those of 1,10-phenanthroline, 2,2′-bipyridine and 4,4′-dimethyl-2,2′-bipyridine were observed at δ 5.5-8.8, 5.4-7.2 and 3.2-5.8 ppm, respectively. Upon complex formation, all signals shifted downfield due to coordination-induced deshielding. A prominent signal at δ 9.7 ppm was assigned to the imidazole N–H proton, while resonances at δ 9.0 and 8.9 ppm corresponded to protons

TABLE-1
KEY FT-IR SPECTRAL DATA OF Ru(II) POLYPYRIDYL COMPLEXES

Ligand/Ru complex	ν(C–H)	ν(N–H)	ν(C–N)	ν(C=C)	ν(C=N)	ν(M–N)
PPIP	811	3462	1070	1602	1525	–
Complex **1**	844	3588	1088	1608	1525	622
Complex **2**	830	3589	1086	1629	1526	622
Complex **3**	823	3589	1075	1608	1527	622

adjacent to the coordinating nitrogen atoms. In the ^{13}C NMR spectra, the carbon signals adjacent to the N-donor atoms shifted from δ 151.91 and 148.42 ppm in the ligand to δ 156.57 and 152.37 ppm in the Ru(II) complexes, further supporting metal coordination.

Mass studies: The ESI-MS spectra of the PPIP ligand and its Ru(II) complexes supported the molecular composition. The free ligand displayed a prominent molecular ion peak at *m/z* 366.9, corresponding to the protonated species $[(M+H)]^+$ and confirming its molecular mass. The Ru(II) complexes exhibited characteristic peaks at *m/z* 414.7 (**1**), 390.1 (**2**) and 418.8 (**3**), which were assigned to the respective doubly charged molecular ions. The observed *m/z* values matched well with the calculated compositions and reflected variations in the coordinated ancillary ligands (Table-2). Complex **3** showed the highest *m/z* value, consistent with the incorporation of a methyl substituted phenanthroline moiety. The spectra were dominated by intact molecular ion peaks accompanied by low-intensity fragment ions arising from partial ligand dissociation, a common feature of Ru(II) polypyridyl complexes. The lack of significant signals attributable to uncoordinated PPIP ligand confirmed successful coordination to the Ru center and the formation of the desired complexes.

TABLE-2
MASS SPECTRAL VALUES OF Ru(II) COMPLEXES

Complex	(M+H)	*m/z* value
PPIP	(M+H)	366.9
Complex **1**	M+1	414.7
Complex **2**	M+1	390.1
Complex **3**	M+1	418.8

UV-vis spectroscopy: The UV-vis electronic spectrum of the ligand shows π-π* and n-π* absorption peaks at 226-296 nm range; upon complexation the absorption peaks were shifted slightly towards higher wavelength region (Fig. 1). In case of Ru(II) complexes few bands were observed between 456-468 nm, corresponding to visible metal-ligand charge transfer (MLCT) transitions. The bathochromic and hypochromic shifts were observed in the compounds. From the ligands to Ru(II) complexes there is a shift in the bands towards higher (Table-3). Complexes **1**, **2** and **3** has shown a maximum at 458, 456 and 468 nm, respectively.

Computational study of DNA binding affinity of Ru(II) polypyridyl complexes

Table-4 displays the structural information (M-N bond length and metal-intercalator length) of 3D metal complex conformers. N of the intercalator (PPIP) has a shorter Ru-N bond length than N of the auxiliary ligand. In phen complex (**1**), the Ru-N bond length (N of Intercalator) is short, hence

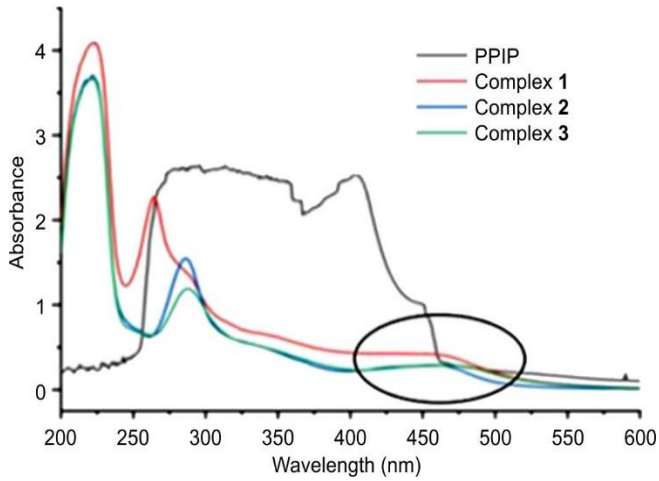

Fig. 1. UV-vis spectrum of PPIP ligand and its Ru(II) complexes

TABLE-3
UV-VIS SPECTRAL DATA OF Ru(II) COMPLEXES

Ligand/Complex	λ_{max}	Band assigned
PPIP	226	$\pi\rightarrow\pi^*$ (INCT)
	296	$n\rightarrow\pi^*$ (INCT)
Complex **1**	224	$\pi\rightarrow\pi^*$ (INCT)
	264	$n\rightarrow\pi^*$ (INCT)
	458	MLCT
Complex **2**	222	$\pi\rightarrow\pi^*$ (INCT)
	286	$n\rightarrow\pi^*$ (INCT)
	456	MLCT
Complex **3**	222	$\pi\rightarrow\pi^*$ (INCT)
	288	$n\rightarrow\pi^*$ (INCT)
	468	MLCT

this complex demonstrates an effective binding with DNA. A short intercalator length for the phen complex (**1**) indicates an effective intercalation. All the complexes bond angles ranged from 89.1º to 94.5º and were closed to octahedral geometry.

Molecular orbitals and energies: The frontier molecular orbitals (HOMO and LUMO) provide useful information about the possible electronic transitions within a molecule. The HOMO–LUMO energy gap is an important parameter for evaluating the chemical reactivity, kinetic stability and electronic properties of a molecule. The HOMO reflects the electron-donating ability of a compound, whereas the LUMO represents its electron-accepting capability. The HOMO energy is associated with the ionization potential (I), while the LUMO energy is related to the electron affinity (A). These descriptors can be estimated directly from the respective HOMO and LUMO energy values.

$$I = -E_{HOMO}$$

$$A = -E_{LUMO}$$

TABLE-4
BOND LENGTHS (Å) OF THE 3D CONFORMERS OF Ru(II) POLYPYRIDYL COMPLEXES

Complex	Metal-intercalator length (Å)	Bond lengths (Å)					
		$M\text{-}N_1{}^a$	$M\text{-}N_2{}^a$	$M\text{-}N_3{}^a$	$M\text{-}N_4{}^a$	$M\text{-}N_5{}^b$	$M\text{-}N_6{}^b$
Complex **1**	15.3465	1.9518	1.9529	1.9532	1.9526	1.9523	1.9525
Complex **2**	15.3739	1.9539	1.9548	1.9510	1.9505	1.9514	1.9514
Complex **3**	15.3535	1.9537	1.9543	1.9506	1.9490	1.9514	1.9524

The data for the HOMO-LUMO gap ($\Delta E/E_g$), ionisation potential and electron affinity of the ligand and its Ru(II) complexes are presented in Table-5. It was observed that the HOMO and LUMO energy levels of the PPIP ligands are lower than those of their corresponding complexes **1-3**. The HOMO-LUMO energy gap of the Ru(II) complexes (complexes **1-3** are in the range of 5.0448 eV to 5.1210 eV, the PPIP ligand is 7.3713 eV) is smaller than that of pure ligands. In general, a smaller HOMO–LUMO energy gap corresponds to higher chemical reactivity and lower kinetic stability. The Ru(II) complexes exhibited lower energy gaps than the free ligand, indicating enhanced electronic activity upon coordination. Among the three complexes, complex **1** displayed the smallest energy gap (E_g), suggesting greater kinetic lability and reactivity. This observation is consistent with the experimental DNA-binding studies, in which complex **1** showed the strongest binding affinity toward DNA.

The 3D contour plots for the electrostatic potential of the free ligands and their Ru(II) complexes are shown in Fig. 2. From these plots, it is observed that the LUMO is predominantly distributed over the Ru(II) center, the ancillary ligands (phen, bpy and dimethyl bpy) and the coordinated imidazole rings. In contrast, the HOMO is mainly localized on the N-phenyl pyrrolidine moiety of the intercalating ligand. This distribution indicates that the Ru(II) center and imidazole rings are the most probable reactive sites involved in electron-accepting processes and molecular interactions (Fig. 3).

Biological and chemical reactivity parameters: The molecular descriptors, including absolute hardness (η), softness (σ), global softness (S), electronegativity (χ), chemical potential (μ), electrophilicity index (ω) and maximum electronic charge transfer (ΔN_{max}), were calculated using eqns. 1-8 and are summarized in Table-6. The calculated HOMO–LUMO energies and associated descriptors indicate that the Ru(II) complexes are more reactive than the free ligand. Among the complexes, the Ru–phen system exhibited the lowest hardness (η), highest electrophilicity (ω), lowest chemical potential (μ) and highest softness (σ), reflecting its superior reactivity. The results highlight the significant influence of the ancillary ligand on the electronic properties, stability, DNA-binding ability and biological activity of Ru(II) polypyridyl complexes [31].

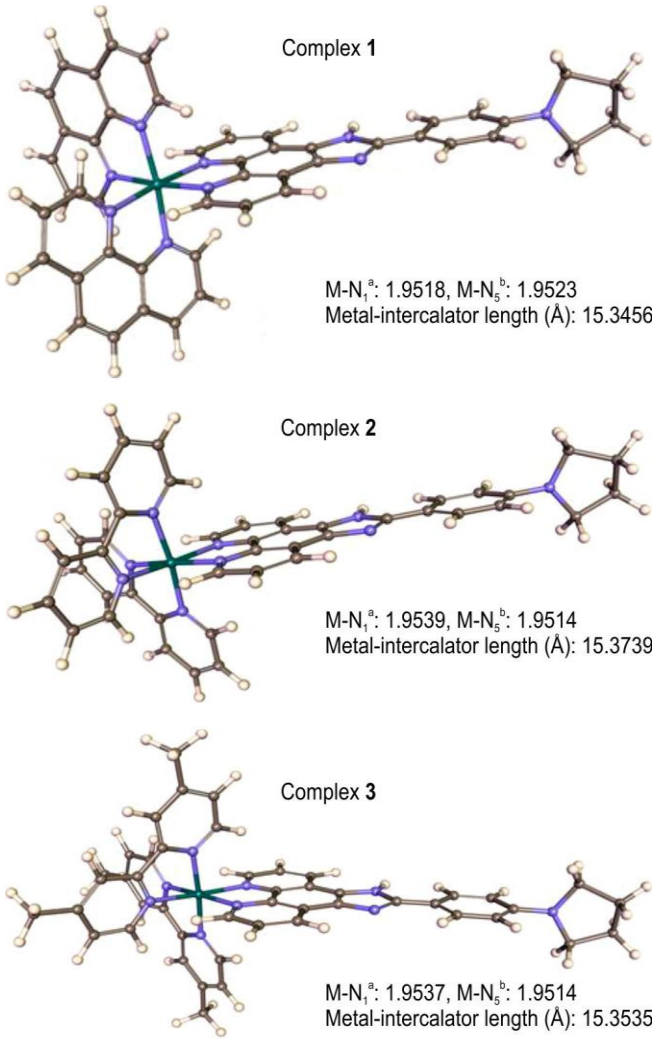

Fig. 2. 3D-dimensional optimised structures of Ru(II) polypyridyl complexes of PPIP ligand, where metal in green, N in blue, C in gray, H in cream colour

$$E_g = E_{LUMO} - E_{HOMO} \quad (1)$$

$$\chi = \frac{E_{LUMO} + E_{HOMO}}{2} \quad (2)$$

TABLE-5
HOMO, LUMO, LUMO-HOMO GAP (ΔE), IP AND EA VALUES OF LIGANDS AND Ru(II) POLYPYRIDYL COMPLEXES

Ligand/metal complex	HOMO (eV)	LUMO (eV)	ΔE (LUMO-HOMO gap) (eV)	Ionisation potential (IP) (eV)	Electron affinity (EA) (eV)
PPIP	-8.2176	-0.8462	7.3713	8.2176	0.8462
Complex **1**	-11.1373	-6.0924	5.0448	11.1373	6.0924
Complex **2**	-11.1781	-6.0648	5.1132	11.1781	6.0648
Complex **3**	-11.0638	-5.9428	5.1210	11.0638	5.9428

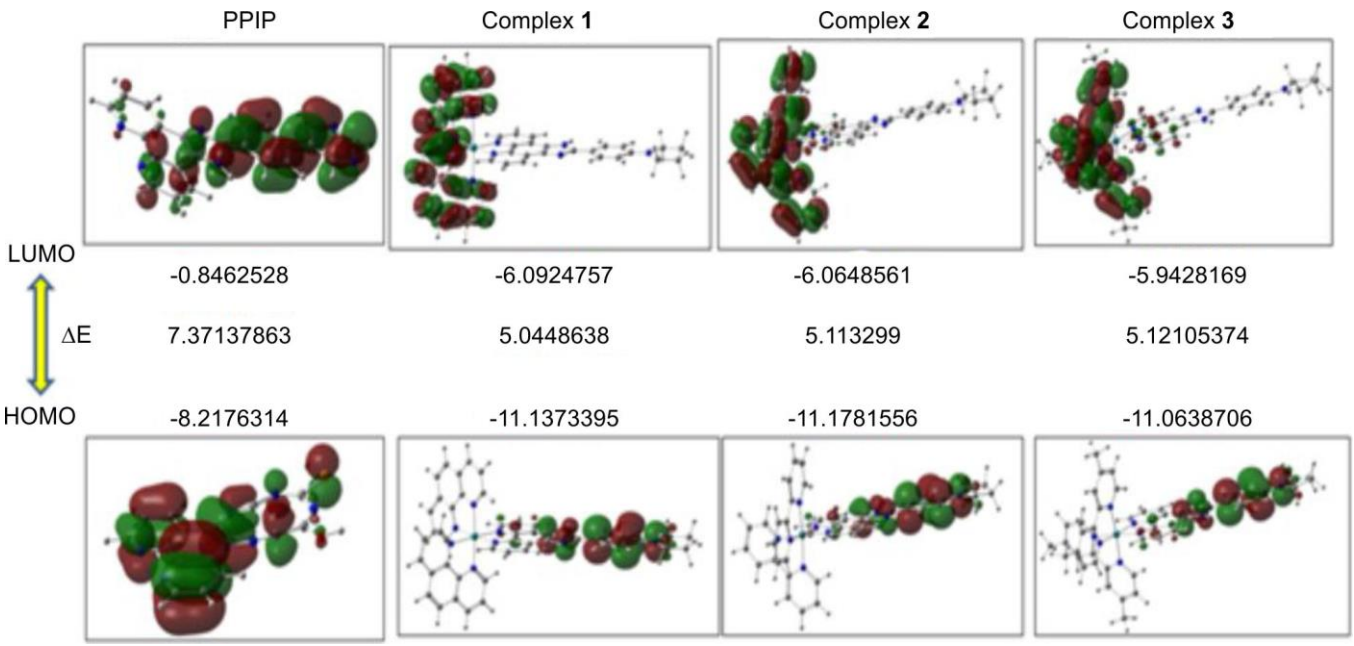

Fig. 3. Electrostatic potential surface (ESP) for PPIP and its Ru(II) complexes

TABLE-6
BIOLOGICAL AND CHEMICAL REACTIVITY PARAMETERS OF SYNTHESISED LIGANDS AND Ru(II) POLYPYRIDYL COMPLEXES

Ligand/metal complex	η	σ	ω	μ	χ	S	ΔN_{max}
PPIP	3.6856	0.2713	2.7862	-4.5319	4.5319	1.8428	1.2296
Complex **1**	2.5224	0.3964	14.7113	-8.6149	8.6149	1.2612	3.4153
Complex **2**	2.5566	0.3911	14.3832	-8.7115	8.7115	1.2333	3.5317
Complex **3**	2.5605	0.3905	14.1195	-8.5033	8.5033	1.2802	3.3209

$$\eta = \frac{E_{LUMO} - E_{HOMO}}{2} \quad (3)$$

$$\sigma = \frac{1}{\eta} \quad (4)$$

$$P_i = -\chi \quad (5)$$

$$S = \frac{1}{2\eta} \quad (6)$$

$$\Omega = \frac{P_i^2}{2\eta} \quad (7)$$

$$\Delta N_{max} = -\frac{P_i}{\eta} \quad (8)$$

Biological studies

DNA interactions

UV-visible absorption studies: The binding capacity and interaction of the Ru(II) complexes with *ct*-DNA were examined by electronic absorption spectroscopy. Absorption spectra were obtained using a Shimadzu UV-vis 2600 spectrophotometer in a Tris-HCl buffer (50 mM NaCl, 5 mM Tris-HCl) at pH 7.2 and 25 ºC. Constant complex concentrations (20 μM) were sustained while varying the amounts of *ct*-DNA by sequential increments of 10 μM to perform absorption titration studies. Generally, when metal complexes intercalate with DNA base pairs, a reduction in colour intensity (hypochromism) occurs, accompanied by a slight shift towards longer wavelengths (red shift) [32]. Eqn. 1 was used to calculate the intrinsic binding constants (K_b).

$$\frac{[DNA]}{(\varepsilon_a - \varepsilon_f)} = \frac{[DNA]}{(\varepsilon_b - \varepsilon_f)} + \frac{1}{K_b(\varepsilon_b - \varepsilon_f)} \quad (1)$$

where ε_a, ε_b and ε_f represent the absorption extinction coefficient (A_{obsd}/[complex]), the extinction coefficient of complex in the fully bound form and the extinction coefficient of the free complex, respectively and [DNA] is the concentration of DNA.

The plots depicting the ratio of DNA concentration to the difference in absorbance between DNA and the solvent ($\varepsilon_a - \varepsilon_f$) *vs.* DNA concentration exhibited linear relationships. The results show that all complexes exhibit strong DNA bin-ding, with complex **1** showing the highest affinity, followed by complexes **2** and **3** (Fig. 4). This stronger binding is attributed to the increased planarity of the ancillary phen ligand. In contrast, methyl substitutions at the 4,4′-positions of dmb ligand introduce steric hindrance, reducing the binding constant. The K_b values follow the order: **1** > **2** > **3** (Table-7).

TABLE-7
BINDING CONSTANTS (K_b) AND K_{sv} VALUES
OF THE Ru(II) POLYPYRIDYL COMPLEXES

Complex	K_b from absorption (M^{-1})	K_b from emission (M^{-1})	K_{sv} from quenching
Complex **1**	3.9×10^5	4.2×10^5	5.3×10^5
Complex **2**	3.4×10^5	3.7×10^5	3.9×10^5
Complex **3**	3.1×10^5	3.3×10^5	3.5×10^5

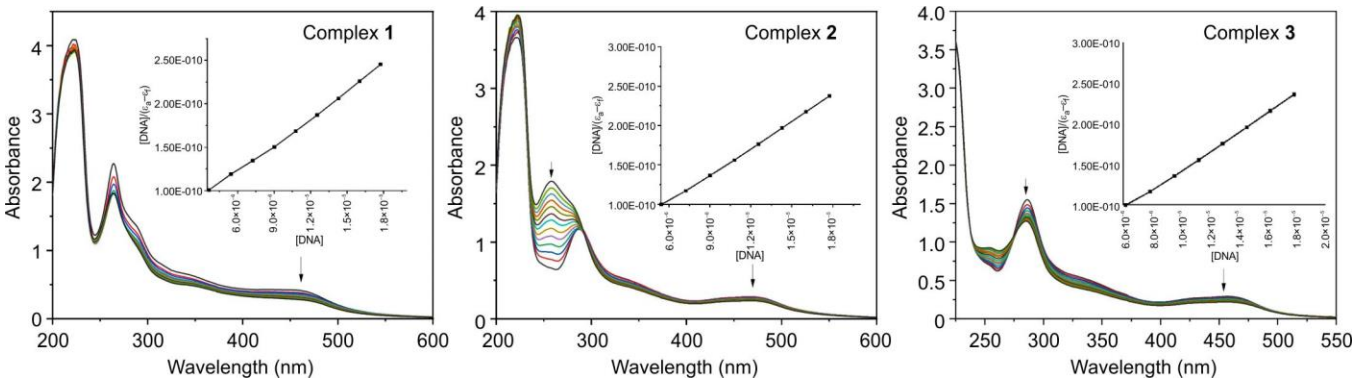

Fig. 4. Absorption studies of Ru(II) polypyridyl complexes in Tris-HCl buffer upon addition of *ct*-DNA. Arrow shows hypochromic and bathochromic shifts upon increase of DNA concentration. Inserted plot, [DNA]/(ε_a-ε_f) *versus* [DNA] for the titration of DNA with Ru(II) complex, which gives intrinsic binding constant (K_b)

Fluorescence studies:

$$C_b = C_t\left(\frac{F - F_o}{F_{max} - F_o}\right) \quad (2)$$

The luminescence titrations were carried out similar to absorption titrations using the Tris-HCl buffer. The complexes were stimulated at 458, 456 and 468 nm and emissions were detected at 601, 610 and 617 nm, respectively. To a fixed metal concentration (20 μL), different concentrations (10-120 μL) of DNA were added. As the concentration of *ct*-DNA grew, so did the strength of the emissions, which eventually plateaued. The fraction of the Ru(II) compound bound was calculated from eqn. **2**, where C_t is the total complex concentration, F is the observed fluorescence emission intensity at a given DNA concentration, F_0 is the intensity in the absence of DNA and F_{max} is when the complex is maximum bound to DNA. The fluorescence binding constant (K_b) of complexes **1**, **2** & **3** was obtained from Scatchard equation and data were cast into the Scatchard plot of r/C_f against r. Where r is the C_b/[DNA] and C_f is the concentration of the free complex [33]. The K_b values for complexes **1**, **2** and **3** were found to be 4.2 × 10^5 M^{-1}, 3.7 × 10^5 M^{-1} and 3.3 × 10^5 M^{-1}, respectively (Table-7). The variation in K_b values is attributed to differences in the ancillary ligands. Complex **3** exhibits a lower K_b value due to the steric hindrance.

Quenching studies: The capacity of Ru(II) complexes to bind DNA was further investigated through fluorescence quenching experiments. Different concentrations of the Ru(II) complexes were added to an ethidium bromide and *ct*-DNA solution to allow for reaction. The concentrations of the Ru(II) complexes was kept between 10 and 100 μM, whereas ethidium bromide and *ct*-DNA were kept at 40 and 130 μm, respectively. Upon incremental addition of the Ru(II) complexes, a progressive decrease in the emission intensity of the EB-DNA system was observed, as indicated by the arrow in the spectra, suggesting displacement of intercalated ethidium bromide from the DNA base pairs. The fluorescence emission spectra were recorded in the range of 560-760 nm with a maximum emission at 620 nm (Fig. 5). To investigate the quenching mechanism, the Stern-Volmer equation [$I_o/I = 1 + K_{sv}\cdot r$], where I and I_o stand for fluorescence intensities in the presence and absence of complexes, respectively and K_{SV} linear Stern-Volmer quenching constant based on the ratio of r_{EB} (the ratio of the bound concentration of EB to the concentration of DNA) and total concentration of the complex to that of DNA, is r thus the spectra were examined.

Analysis of the quenching data afforded K_{SV} values of 5.3 × 10^5, 3.9 × 10^5 and 3.5 × 10^5 M^{-1} for complexes **1**, **2** and **3**, respectively (Table-7). The relatively high quenching constants indicate efficient interaction of the complexes with DNA, consistent with a strong binding affinity and a probable intercalative binding mode. The binding strength follows the order: Complex **1** > Complex **2** > Complex **3**, which is in agreement with the calculated DNA-binding constants.

Viscosity: To further elucidate the DNA-binding mode of the Ru(II) complexes, viscosity measurements were carried out using *ct*-DNA as a hydrodynamic probe. Viscosity studies are considered one of the most reliable methods for distinguishing intercalative interactions, as the insertion of a molecule between adjacent DNA base pairs extends the DNA helix and consequently increases the viscosity of the solution. The relative viscosity of *ct*-DNA was measured in the absence and presence of the synthesized Ru(II) complexes and the results are presented in Fig. 6. Upon gradual addition of the Ru(II) complexes, a modest but consistent increase in DNA viscosity was observed. Although the magnitude of the increase was lower than that produced by the classical intercalator ethidium bromide, the trend clearly suggests partial intercalation of the complexes into the DNA base stack. The observed viscosity enhancement followed the order ethidium bromide > **1** > **2** > **3**, indicating that complex **1** exhibits the strongest interaction with DNA among the synthesised complexes. These findings provide strong evidence for an intercalative mode of DNA binding and are in good agreement with the results obtained from UV-Vis absorption and fluorescence displacement studies. The consistency among these independent techniques confirms the significant affinity of the complexes toward DNA and supports the proposed binding mechanism.

Photocleavage studies: The DNA cleavage activity of Ru(II) complexes was investigated using agarose gel electrophoresis with pBR322 plasmid DNA. As shown in Fig. 7, untreated DNA (Lane 1) served as the control and displayed the characteristic fast-moving supercoiled form (Form I). The photolysis experiment was performed by incubating pBR322

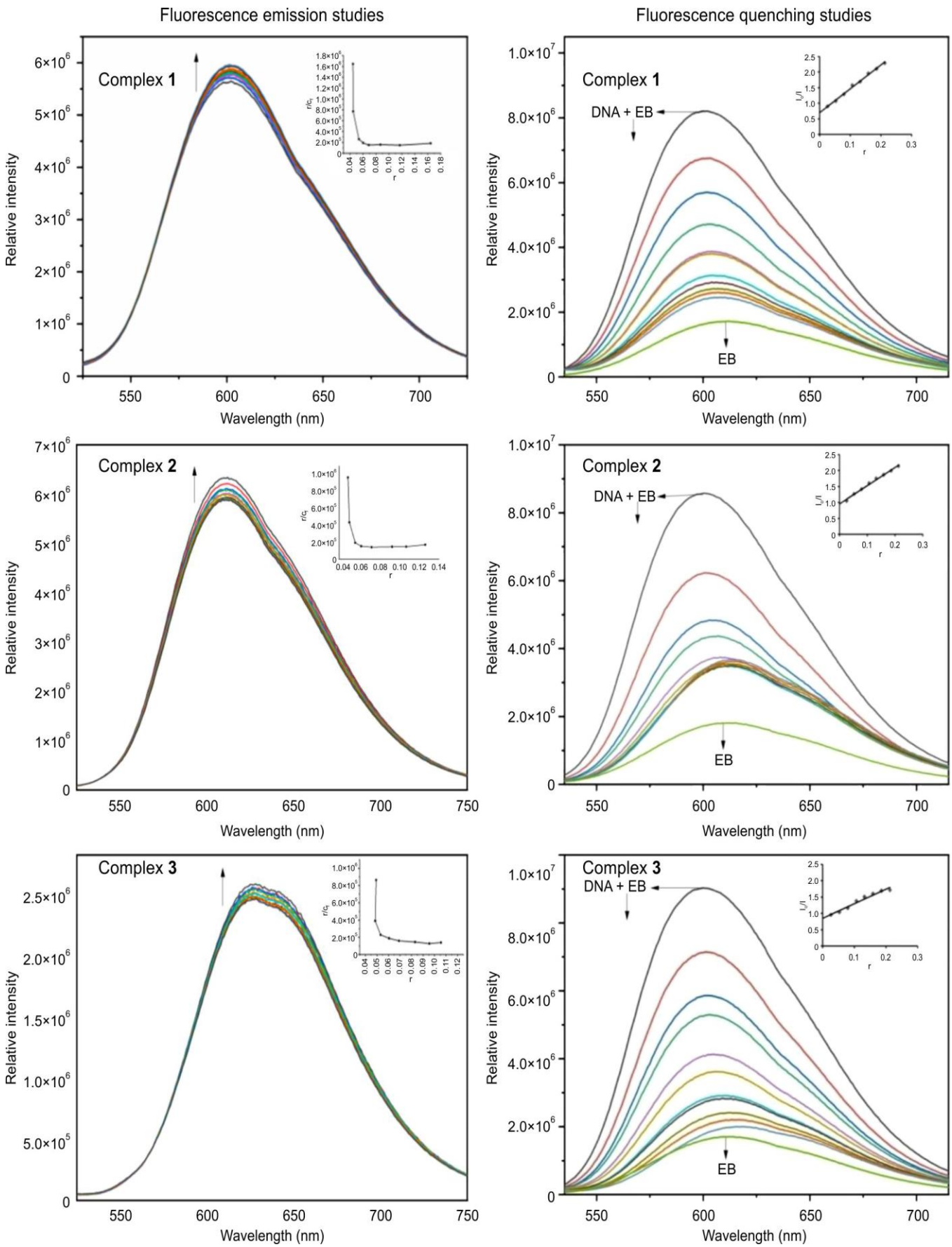

Fig. 5. Fluorescence emission and quenching spectra of Ru(II) PPIP polypyridyl complexes in Tris-HCl buffer

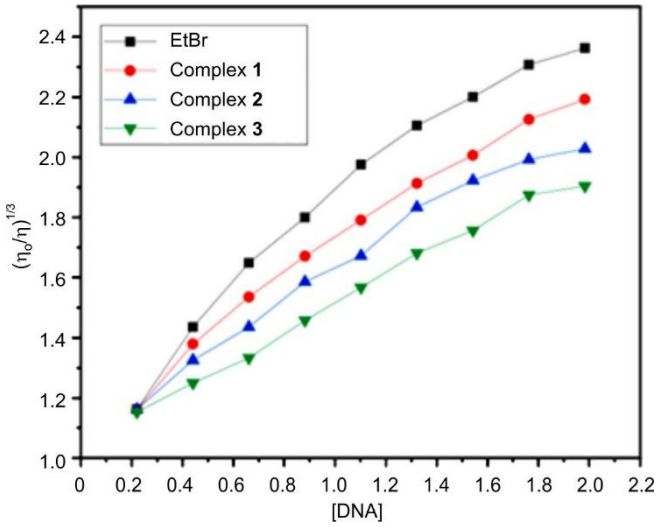

Fig. 6. Viscosity studies of Ru(II) PPIP complexes in Tris-HCl buffer with increasing concentration of complexes and ethidium bromide (EtBr) on the relative viscosity of *ct*-DNA at room temperature

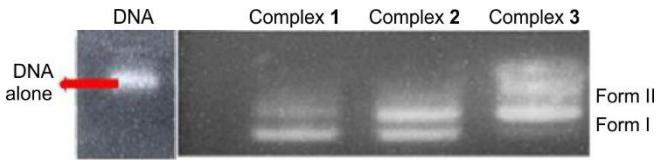

Fig. 7. Photocleavage images of Ru(II) PPIP complexes in agarose gel electrophoresis of pBR322 DNA alone and in the presence of complexes with the concentration range of 20 μM after irradiation at 365 nm for 60 min under UV light

DNA with the Ru(II) complex (20 μM) followed by UV irradiation at 365 nm for 60 min. After treatment, the appearance of slower-moving open circular DNA (Form II) indicated single strand cleavage (nicking) of the plasmid. The conversion of supercoiled DNA to relaxed forms demonstrates that the Ru(II) complexes possess significant photoinduced DNA cleavage activity confirmed their ability to effectively damage plasmid DNA under irradiation conditions.

Antimicrobial activity: The antimicrobial activity was evaluated using the pour plate method. Complexes **1-3** were screened *in vitro* at concentrations of 0.5 and 1 mg mL^{-1} against selected Gram-positive bacteria (*Staphylococcus aureus* and *Bacillus subtilis*), Gram-negative bacteria (*Escherichia coli* and *Klebsiella pneumoniae*) and fungal strains (*Aspergillus niger* and *Candida albicans*). The results (Table-8) revealed that the Ru(II) complexes exhibited higher antimicrobial activity than the free ligand. The enhanced biological activity upon complexation may be explained by Overtone's concept [34] of cell permeability and Tweedy's chelation theory [35], according to which chelation reduces the polarity of the metal ion through partial sharing of its positive charge with donor atoms. This increased lipophilicity facilitates the penetration of the complexes through microbial cell membranes, thereby improving their antimicrobial efficacy.

Cytotoxicity: The cytotoxicity of the compounds were tested by MTT assay to evaluate the proliferation activities of complexes against MCF-7 cell line comparison with doxorubicin positive control. The cytotoxic activity of the ligand and Ru(II) complexes against MCF-7 cells is shown in Fig. 8. The complexes exhibited greater anticancer activity than the free ligand, indicating that coordination to Ru(II) enhances biological efficacy, although their activity remained lower than that of the standard drug doxorubicin (Table-9). The improved potency of the Ru(II) complexes may be attributed to

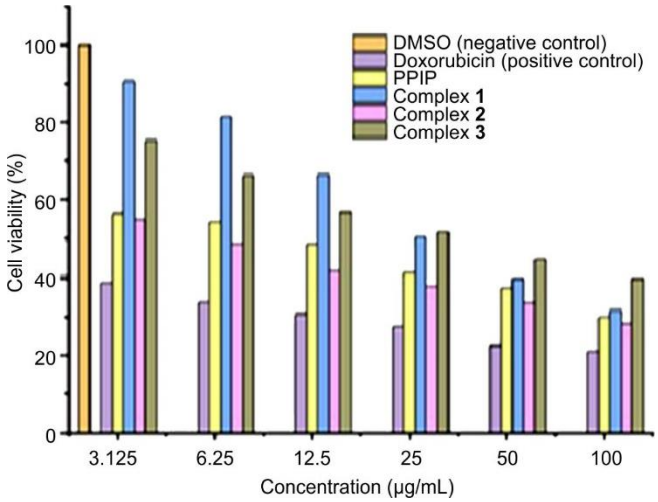

Fig. 8. Cell viability of MCF-7 (human breast cancer) cell line *in vitro* treatment with doxorubicin (positive control) and Ru(II) complexes **1-3**. Every data point is the average ± standard error derived from a minimum of three separate experiments. Negative control (untreated cells) considered as 100% of viable cells

TABLE-9
IC_{50} VALUES OF LIGAND/COMPLEXES (**1-3**) AGAINST MCF-7 CELL LINES

Ligand/complex	IC_{50} value
PPIP	18.76 ± 0.51
Complex **1**	13.53 ± 0.36
Complex **2**	14.89 ± 0.13
Complex **3**	16.93 ± 0.36

TABLE-8
ANTIMICROBIAL ACTIVITY DATA OF Ru(II) COMPLEXES **1-3**

Complex	Zone of inhibition (mm)					
	Gram-positive bacterial pathogens		Gram-negative Bacterial pathogens		Fungal pathogens	
	Staphylococcus aureus	*Bacillus subtilis*	*Escherichia coli*	*Klebsiella pneumoniae*	*Candida albicans*	*Aspergillus niger*
PPIP	6	4	4	4	4	4
Complex **1**	12	10	10	10	08	10
Complex **2**	08	08	12	12	12	10
Complex **3**	08	12	12	12	12	10
Standard	16	14	12	12	12	12

their increased lipophilicity, which promotes cellular uptake. A concentration dependent variation in cell viability was observed. Among the complexes, complex **1** showed higher cell viability than complexes **2** and **3**, likely due to the greater planarity of the phenanthroline ancillary ligand.

Conclusion

In summary, three biologically active Ru(II) complexes (complexes **1-3**) incorporating the novel PPIP ligand were successfully synthesised and characterised. Spectroscopic analyses confirmed an octahedral coordination environment around the Ru(II) center. DNA-binding studies revealed strong interactions with *ct*-DNA, with the binding affinity following the order complex **1** > complex **2** > complex **3**. Complex **1** exhibited the strongest DNA affinity, which may be associated with its electronic properties, with a favourable HOMO–LUMO energy gap and increased molecular softness. All complexes induced cleavage of plasmid DNA, converting the supercoiled Form I into the open circular Form II, demonstrating effective nuclease-like activity. The complexes also displayed enhanced antimicrobial and antitumor activities compared to the free ligand, highlighting the beneficial effect of Ru(II) coordination on biological performance. UV-Vis absorption, fluorescence quenching and viscosity measurements suggest that the Ru(II) complexes interact with DNA predominantly through an intercalative mode. Significant hypochromism and bathochromic shifts in the MLCT bands, efficient fluorescence quenching and increased DNA viscosity support this binding mechanism.

ACKNOWLEDGEMENTS

The authors are thankful to the Head, Department of Chemistry and The Principal, University College of Science, Saifabad, Osmania University, Hyderabad for providing the research facilities to carry out this work.

CONFLICT OF INTEREST

The authors declare that there is no conflict of interests regarding the publication of this article.

DECLARATION OF AI-ASSISTED TECHNOLOGIES

During the preparation of this manuscript, the authors used an AI-assisted tool(s) to improve the language. The authors reviewed and edited the content and take full responsibility for the published work.

REFERENCES

1. S. Ramasamy and A.T. Rajan, *J. Fluoresc*., **32**, 1873 (2022); https://doi.org/10.1007/s10895-022-02987-2
2. M. Bal, M. Tümer and M. Köse, *J. Fluoresc*., **32**, 2237 (2022); https://doi.org/10.1007/s10895-022-03007-z
3. A.L. Berhanu, I. Mohiuddin, A.K. Malik and J.S. Aulakh, *J. Fluoresc*., **34**, 2093 (2024); https://doi.org/10.1007/s10895-023-03435-5
4. G. Ramesh, S. Daravath, K. Jagadesh Babu, R. Dharavath, A. Ranjan, D. Ayodhya, and Shivaraj, *J. Fluoresc*., **35**, 2087 (2024); https://doi.org/10.1007/s10895-024-03657-1
5. H. Kargar, M. Fallah-Mehrjardi, R. Behjatmanesh-Ardakani, V. Torabi, K.S. Munawar, M. Ashfaq and M.N. Tahir, *J. Mol. Struct*., **1243**, 130782 (2021); https://doi.org/10.1016/j.molstruc.2021.130782
6. M.S. More, P.G. Joshi, Y.K. Mishra and P. Khanna, *Mater. Today Chem.*, **14**, 100195 (2019); https://doi.org/10.1016/j.mtchem.2019.100195
7. M.N. Ahamad, K. Iman, M.K. Raza, M. Kumar, A. Ansari, M. Ahmad and M. Shahid, *Bioorg. Chem*., **95**, 103561 (2020); https://doi.org/10.1016/j.bioorg.2019.103561
8. T. Baran, *J. Mol. Struct*., **1141**, 535 (2017); https://doi.org/10.1016/j.molstruc.2017.03.122
9. R. Kargar, M. Fallah-Mehrjardi, R. Behjatmanesh-Ardakani, V. Torabi, K.S. Munawar, M. Ashfaq and M.N. Tahir, *J. Mol. Struct*., **1243**, 130782 (2021); https://doi.org/10.1016/j.molstruc.2021.130782
10. R. Antony, G.L. Tembe, M. Ravindranathan and R.N. Ram, *J. Mol. Catal. A Chem*., **171**, 159 (2001); https://doi.org/10.1016/S1381-1169(01)00092-9
11. S. Bräuchle and H. Huppertz, *J. Solid State Chem*., **253**, 242 (2017); https://doi.org/10.1016/j.jssc.2017.05.044
12. M. Bharathi, S. Indira, G. Vinoth, D.B.C. Leslee and K. Shanmuga Bharathi, *Polyhedron*, **229**, 116188 (2023); https://doi.org/10.1016/j.poly.2022.116188
13. M. Monier, *Int. J. Biol. Macromol*., **50**, 773 (2012); https://doi.org/10.1016/j.ijbiomac.2011.11.026
14. M. Almáši, M. Vilková and J. Bednarčík, *Inorg. Chim. Acta*, **515**, 120064 (2021); https://doi.org/10.1016/j.ica.2020.120064
15. T. Baran, *Int. J. Biol. Macromol*., **127**, 232 (2019); https://doi.org/10.1016/j.ijbiomac.2019.01.046
16. Ö. Özdemir, *J. Mol. Struct*., **1179**, 376 (2019); https://doi.org/10.1016/j.molstruc.2018.11.023
17. M. Pervaiz, I. Ahmad, M. Yousaf, S. Kirn, A. Munawar, Z. Saeed, A. Adnan, T. Gulzar, T. Kamal, A. Ahmad and A. Rashid, *Spectrochim. Acta Part A Mol. Biomol. Spectrosc*., **206**, 642 (2019); https://doi.org/10.1016/j.saa.2018.05.057
18. K. Buldurun, N. Turan, A. Savcı and N. Colak, *J. Saudi Chem. Soc*., **23**, 205 (2019); https://doi.org/10.1016/j.jscs.2018.06.002
19. E. Bagdatli, E. Altuntas and U. Sayin, *J. Mol. Struct*., **1127**, 653 (2017); https://doi.org/10.1016/j.molstruc.2016.08.026
20. M.M. Abd-Elzaher, A.A. Labib, H.A. Mousa, S.A. Moustafa, M.M. Ali and A.A. El-Rashedy, *Beni-Suef Univ. J. Basic Appl. Sci.*, **5**, 85 (2016); https://doi.org/10.1016/j.bjbas.2016.01.001
21. H.M. Southam, J.A. Butler, J.A. Chapman and R.K. Poole, *Adv. Microb. Physiol*., **71**, 1 (2017); https://doi.org/10.1016/bs.ampbs.2017.03.001
22. M.D. Hall, H.R. Mellor, R. Callaghan and T.W. Hambley, *J. Med. Chem*., **50**, 3403 (2007); https://doi.org/10.1002/chin.200744228
23. W.H. Ang, I. Khalaila, C.S. Allardyce, L. Juillerat-Jeanneret and P.J. Dyson, *J. Am. Chem. Soc*., **127**, 1382 (2005); https://doi.org/10.1021/ja0432618
24. P. Heringová, J. Woods, F.S. Mackay, J. Kašpárková, P.J. Sadler and V. Brabec, *J. Med. Chem*., **49**, 7792 (2006); https://doi.org/10.1021/jm0606692
25. E. Hillard, A. Vessières, L. Thouin, G. Jaouen and C. Amatore, *Angew. Chem. Int. Ed*., **45**, 285 (2006); https://doi.org/10.1002/anie.200502925
26. C. Scolaro, A. Bergamo, L. Brescacin, R. Delfino, M. Cocchietto, G. Laurenczy, T.J. Geldbach, G. Sava and P.J. Dyson, *J. Med. Chem*., **48**, 4161 (2005); https://doi.org/10.1021/jm050015d.
27. M.R. Gill, *RSC Med. Chem.*, **17**, 2726 (2026); https://doi.org/10.1039/D6MD00154H
28. M. Malagarriga Pérez and L. González, *Phys. Chem. Chem. Phys.*, **26**, 27116 (2024); https://doi.org/10.1039/D4CP02018A
29. V. Rajendiran, R. Karthik, M. Palaniandavar, H. Stoeckli-Evans, V.S. Periasamy, M.A. Akbarsha, B.S. Srinag and H. Krishnamurthy, *Inorg. Chem*., **46**, 8208 (2007); https://doi.org/10.1021/ic700755p

30. N. Jyothi, S. Daravath, M. Swathi, K. Jagadeshbabu, N. Ganji and Shivaraj, *J. Mol. Struct.*, **1295**, 136529 (2024); https://doi.org/10.1016/j.molstruc.2023.136529
31. M. Swathi, D.S. Shankar, S. Daravath, N. Ganji, P.V. Anantha Lakshmi and Shivaraj, *Inorg. Chem. Commun.*, **153**, 110826 (2023); https://doi.org/10.1016/j.inoche.2023.110826
32. A. Patra, H. Puschmann and S.C. Manna, *Polyhedron*, **201**, 115146 (2021); https://doi.org/10.1016/j.poly.2021.115146
33. C.N. Baker, S.A. Stocker, D.H. Culver and C. Thornsberry, *J. Clin. Microbiol.*, **29**, 533 (1991); https://doi.org/10.1128/JCM.29.3.533-538.1991
34. B.G. Tweedy, *Phytopathology*, **55**, 910 (1964).
35. J. Parekh, P. Inamdhar, R. Nair, S. Baluja and S. Chanda, *J. Serb. Chem. Soc.*, **70**, 1155 (2005); https://doi.org/10.2298/JSC0510155P